ACSNANO

www.acsnano.org

ARTICLE

Ultrastable Glassy Polymer Films with an Ultradense Brush Morphology

Biao Zuo,* Cheng Li, Quanyin Xu, Katelyn Randazzo, Naisheng Jiang, Xinping Wang,* and Rodney D. Priestley*

Cite This: *ACS Nano* 2021, 15, 9568–9576

Read Online

ACCESS | Metrics & More | Article Recommendations | Supporting Information

ABSTRACT: **Glassy polymer films with extreme stability could enable major advancements in a range of fields that require the use of polymers in confined environments. Yet, from a materials design perspective, we now know that the glass transition temperature (T_g) and thermal expansion of polymer thin films can be dramatically different from those characteristics of the bulk, *i.e.*, exhibiting confinement-induced diminished thermal stability. Here, we demonstrate that polymer brushes with an ultrahigh grafting density, *i.e.*, an ultradense brush morphology, exhibit a significant enhancement in thermal stability, as manifested by an exceptionally high T_g and low expansivity. For instance, a 5 nm thick polystyrene brush film exhibits an ∼75 K increase in T_g and ∼90% reduction in expansivity compared to a spin-cast film of similar thickness. Our results establish how morphology can overcome confinement and interfacial effects in controlling thin-film material properties and how this can be achieved by the dense packing and molecular ordering in the amorphous state of ultradense brushes prepared by surface-initiated atom transfer radical polymerization in combination with a self-assembled monolayer of initiators.**

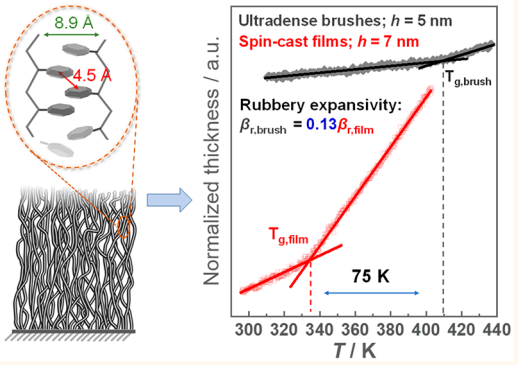

KEYWORDS: *ultrastable polymer glasses, glass transition, thermal expansion, polymer brushes, thin polymer films*

A polymer brush is a thin film, in which the morphology is characterized by the chemical grafting of each chain at one end to a solid surface. The brush morphology, which is different from that of thin films prepared by spin coating, has good ability to modify the interfacial properties of the substrate, including wettability and adhesion.[1,2] A predominant feature of polymer brushes is that the areal grafting density (σ_P) strongly influences structure and properties.[3,4] When $\sigma_P > 2R_g^{-2}$, where R_g is the radius of gyration of the unperturbed chain, the chains are in the "brush" regime, which is characterized by their extension in the direction perpendicular to the substrate.[3,4] In this regime, brushes can exhibit a variety of enhancements in physical properties relative to those of other film morphologies, *e.g.*, higher T_g,[5] enhanced modulus,[6] reduced friction,[7] resistance against compression,[8] and reduction in swelling capacity.[9] Notably, the changes in material properties occur even though $\sigma_P \ll \sigma_{P,max}$, in which $\sigma_{P,max}$ is defined as the theoretical maximum brush density assuming a fully stretched chain conformation.[10] As an example, for polystyrene (PS) and poly(methyl methacrylate) (PMMA), two thoroughly investigated brushes, the typical σ_P reported is 0.1−0.7 nm^{-2},[3,5,10,11] which is far below the $\sigma_{P,max}$ of 1.45 and 1.52 nm^{-2} for PS and PMMA, respectively.[10] In other words, the reduced grafting density ($\sigma_p^* = \sigma_P/\sigma_{P,max}$) is far below unity. It has been shown theoretically that when σ_p^* approaches unity (*i.e.*, the theoretical maximum of σ_p)—here defined as the definition of an ultradense brush—a well-ordered film structure with higher-order intermolecular interactions exists,[12−14] which may alter thermodynamic properties of the tethered chains and even drive them into the crystal state.[12] Since the discovery of polymer brushes, there remain significant efforts[4,10,15] to prepare such polymers with ultradense brush morphology (see Figure S1). The formation of polymer brushes with an ultrahigh grafting density will allow for investigations on how this distinctive morphology, characterized by hyperefficient chain packing, can lead to transformative changes in material properties.

The two primary approaches developed to generate polymer brushes are "grafting-to" and "grafting-from" methods.[16−18]

Received: November 16, 2020
Accepted: May 18, 2021
Published: May 25, 2021

https://doi.org/10.1021/acsnano.0c09631
ACS Nano 2021, 15, 9568−9576

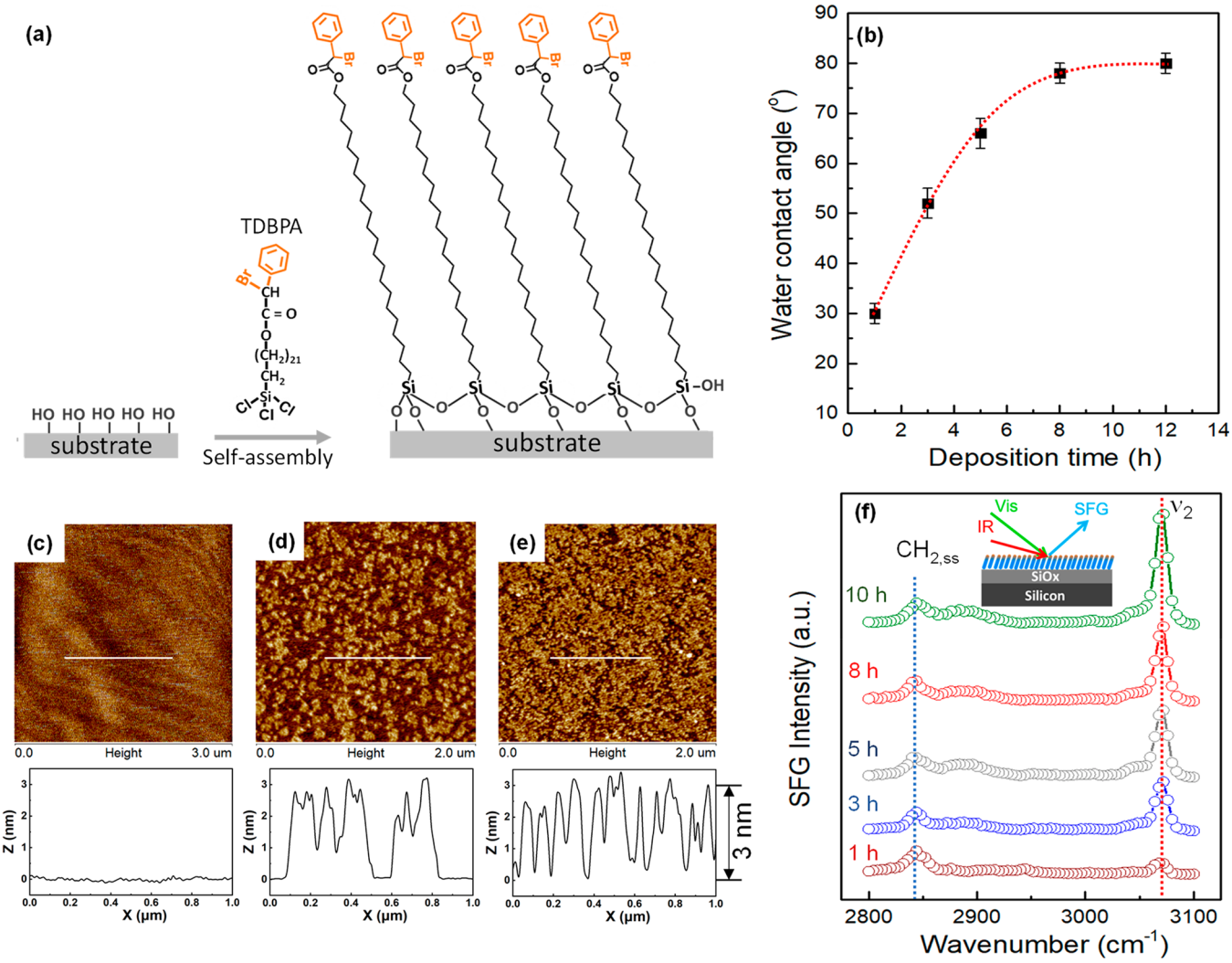

Figure 1. (a) Schematic diagram of the process of attaching initiators atop Si *via* the self-assembly of a TDBPA monolayer with a long alkyl spacer and the local structure of the TDBPA molecules within the SAM. (b) The water contact angle of TDBPA SAMs obtained as a function of deposition time. The dashed red line serves as a guide to the eye. AFM snapshots of the surface topography and profiles of (c) the bare Si substrate and (d,e) SAM. SAMs in panels (d) and (e) were prepared using reaction times of 3 and 8 h, respectively. (f) SFG spectra of the TDBPA SAMs (the inset shows the configuration of SFG measurements).

The former, in which premade polymer chains are grafted to a surface, cannot produce a dense brush, as the depletion of active sites and steric hindrance restricts the probability of late-arriving polymer chains from grafting to the surface.[16] Although σ_p can be pushed higher using an assembled single-crystal polymer,[15] this self-assembly assisted graft-to method[15] is limited to semicrystalline polymers and brush layers with thicknesses below 5 nm. The latter method, in which polymer chains are polymerized from the surface of active sites, has produced brushes with higher grafting densities due to the reduced effects of steric hindrance.[3,16] However, the σ_p* of the bushes prepared by the "grafting-from" method is still relatively low, generally below 0.6 (see a summary of literature values of σ_p* in Figure S1 in SI). To our knowledge, the highest σ_p* achieved is 0.77 *via* living free radical polymerization from a polymer substrate embedded with abundant initiators.[19] Fundamental to making an ultrahigh grafting density brush by the "grafting-from" approach is the requirement of near-simultaneous chain initiation from a high uniform density of initiators, followed by slow and constant growth.

The formation of ultradense polymer brushes may find a relation to the emerging field of ultrastable glasses.[20−22] An enhanced T_g and reduced thermal expansion (β) signify increased kinetic and thermal stability of the glassy materials, as higher temperatures are required to dislodge the molecules from the glassy state,[20−22] and the material dimensions are much more stable against temperature variations. The overcrowding and anisotropic structure (*e.g.*, chain stretching) of ultradense brushes would promote favorable molecular packing and ordering, thus facilitating the formation of ultrastable glass.[23] Despite both theoretical[3,4,24,25] and experimental[3,4,12,26] progress in understanding the properties of polymer brushes, the field still lacks a direct measurement of the glass transition dynamics and thermal stability of brushes in the ultradense state. A relatively minor T_g increase with respect to the bulk value was reported for brush films with moderate σ_p* (*i.e.*, 0.4−0.6); T_g increased ~10 ± 5 K for 10 nm thick brush films,[5,27−29] and no change in β[27] was reported. The enduring barrier impeding the characterization and understanding of the stability of ultradense glassy brush films has been the challenge to produce them. Overcoming this

https://doi.org/10.1021/acsnano.0c09631
ACS Nano 2021, 15, 9568−9576

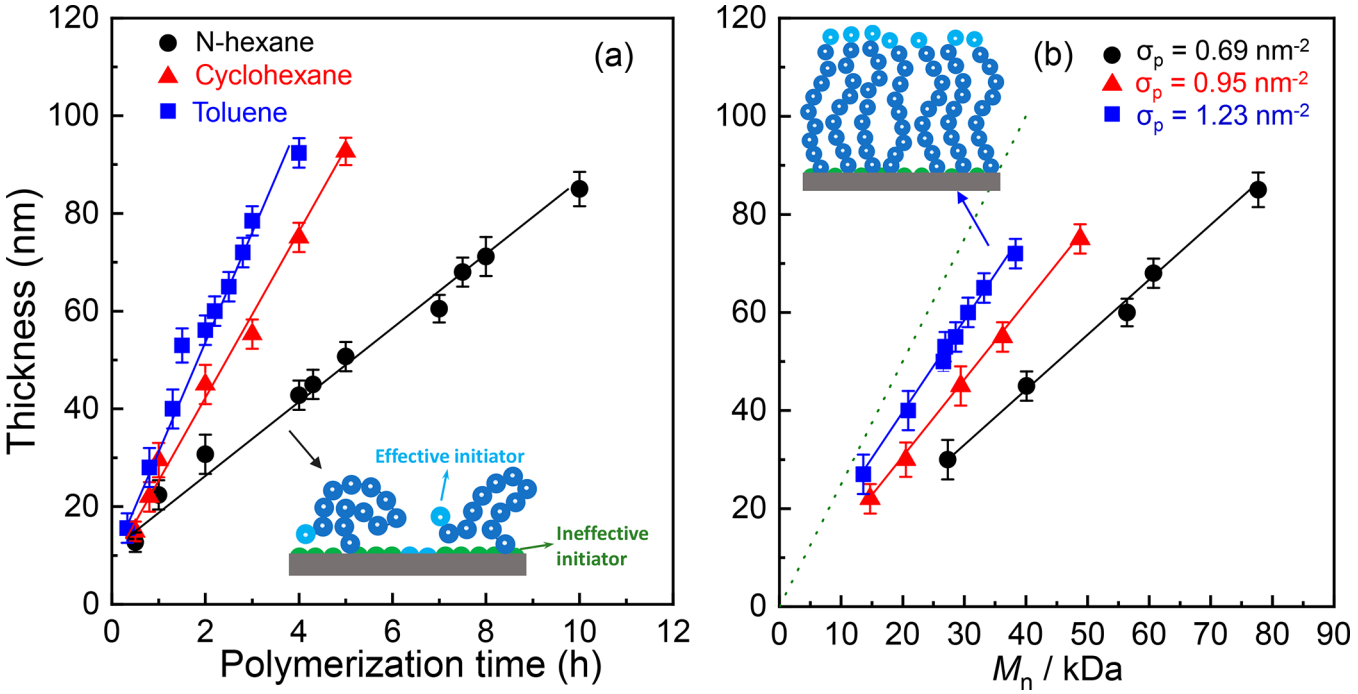

Figure 2. (a) Thickness of dry PS brushes as a function of polymerization time in different solvents. (b) Thickness of dry brushes as a function of the corresponding M_n. The green dotted line represents the theoretical thickness of PS brushes assuming an all-*trans* conformation, *i.e.*, $\sigma_{P,max}$. The insets schematically show the conformations of brush chains in different solvents, which impact grafting density.

challenge holds promises for a conceptual leap in the growing field of ultrastable glassy films and also to advance insights into the thermal stability of confined polymers and how the film morphology influences such behavior.

Here, ultradense brushes of PS with $\sigma_P = 1.23 \pm 0.04$ nm^{-2}, which corresponds to a σ_p* of 0.85—the highest value reported thus far for a polymer brush (Figure S1 in the SI)—were synthesized by surface-initiated controlled/living radical polymerization—atom transfer radical polymerization (SI–ATRP) with good control of the chain growth. The formation of the ultradense brushes was enabled by the self-assembly of a bifunctional initiator [22-(trichlorosilyl) docosyl 2-bromo-2-phenylacetate; TDBPA; see structure in Figure 1a] composed of a silane group at one end and a 2-bromo-2-phenylacetate (BPA; initiating groups for SI–ATRP) at the other—designed with a long alkyl chain to promote ordering into a crystalline monolayer atop silicon substrates. The results can be understood by considering the surface density of the initiator, BPA, and its superhigh reaction rate constant (k) $\approx 5.2 \times 10^3$ m^{-1}s^{-1},[30,31] critically combined with the solubility of the polymerizing chain in the reaction medium. We found that the ultradense nature of the PS brush had a profound influence on the T_g and β of the film. An increase in T_g of ~75 K and a reduction in rubbery state β by ~87% were observed in the 5 nm thick ultradense brush compared to a spin-cast film of comparable thickness. Hence, ultradense brush films exhibit thermal ultrastability—a highly sought-after feature of organic thin films.

RESULTS AND DISCUSSION

Figure 1a schematically illustrates the attachment of initiators atop Si in the form of a monolayer of self-assembled TDBPA with an extended alkyl spacer (*i.e.*, 22 carbon atoms). The long hydrocarbon spacer, associated with strong intermolecular forces, was added to promote chain alignment and crystallization of the TDBPA self-assembled monolayer (SAM). As shown in Figure 1b, the water contact angle atop the SAM surface increased as a function of deposition time and plateaued at ~80 ± 2° after 8 h of deposition. In comparison, the contact angle of a surface fully occupied by phenyl or Br groups is ~83 ± 5°,[32] which is within error of the SAM. The SAM thickness was determined by AFM topological images, as shown in Figure 1d,e. The average thickness was ~3 ± 0.5 nm, as identified by the cross-sectional profiles, and is close to a TDBPA film's height with an all-*trans* conformation, *i.e.*, 3.2 nm, thus suggesting a tightly packed TDBPA SAM.

The TDBPA monolayer structure was further confirmed by sum-frequency generation (SFG) spectroscopy,[33] a sensitive interfacial characterization technique. Two discernible peaks at 2842 and 3066 cm^{-1} appeared from the symmetric stretching vibrations of CH_2($CH_{2,ss}$) in the backbone and ν_2 vibrations of phenyl groups[34,35] exposed at the SAM surface, respectively, as shown in Figure 1f. The $CH_{2,ss}$ peak is due to *gauche* defects in the monolayer[35] and indicates distortion and disorder of the long hydrocarbon chains within the monolayer. However, the intense ν_2 peak, which grows as a function of deposition time, is a pronounced spectral manifestation of the formation of a closely packed all-*trans* TDBPA monolayer, in which the phenyl groups are oriented nearly perpendicularly to the surface. The relative intensity of the ν_2 peak to the $CH_{2,ss}$ peak is thus related to the degree of molecular ordering in the SAM. When the deposition time exceeds 8 h, an intensive ν_2 peak dominates the spectrum, reinforcing the idea of forming an ordered SAM consisting of extended TDBPA molecules, which exposes all the active initiating groups of BPA toward the air interface, as shown in Figure 1(a). We note that alkyl-silane chains with greater than 18 carbon atoms form a well-assembled hexagonal crystalline monolayer[36] and that the

https://doi.org/10.1021/acsnano.0c09631
ACS Nano 2021, 15, 9568–9576

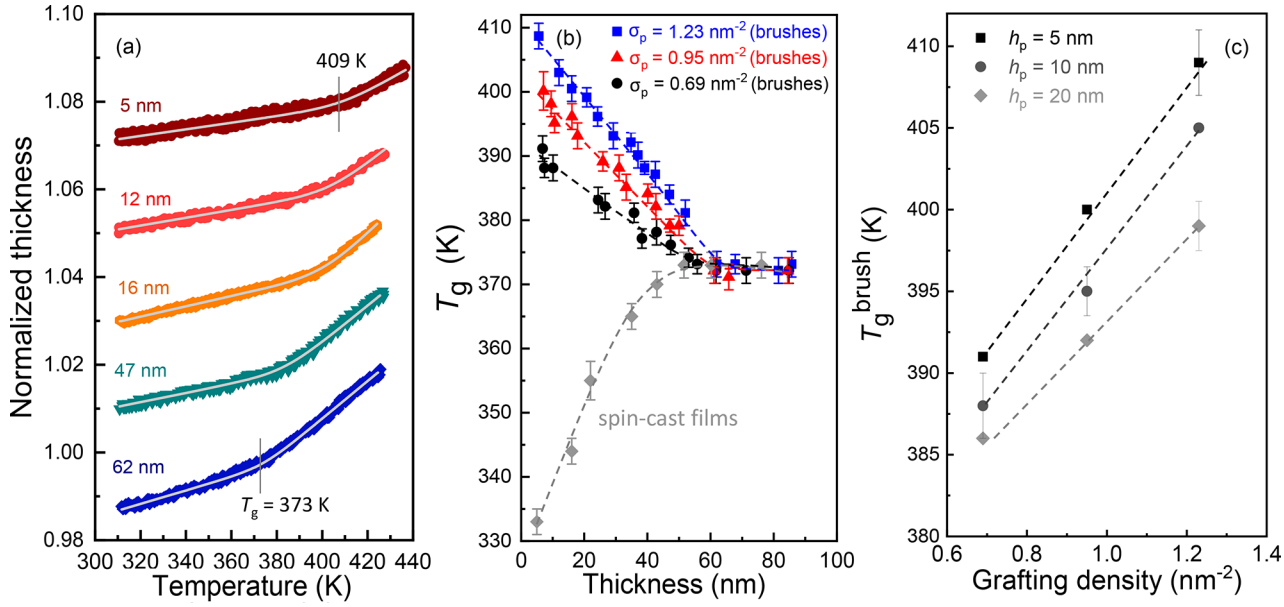

Figure 3. (a) Temperature dependence of normalized thickness for ultradense PS brushes (σ_p = 1.23 nm^{-2}). (b) The relationship between T_g *vs.* thickness of the PS brush and spin-coated films. (c) T_g of PS brush (T_g^{brush}) as a function of the grafting density. The curves in panel (a) were vertically shifted for clarity. Data points in (c) without error bars were obtained by reading off the dash lines in (b).

propensity of self-assembly increases with an increase in the alkyl chain length.[36,37] The introduction of phenyl terminal groups does not disrupt the crystalline structure,[38] such that the ordered structure of TDBPA is retained, as confirmed by data in Figure 1. Based on the molecular area of aromatic groups in a perpendicularly oriented crystalline monolayer (*i.e.*, 0.23 nm^2),[39] the area density of BPA atop the SAM surface was estimated to be about 4.6 nm^{-2}—a value exceedingly higher than the $\sigma_{p,max}$ of PS brushes, *i.e.*, 1.45 nm^{-2}. Additionally, the initiating group of BPA has a rate constant more than 2000 times that of the traditionally used initiator (*i.e.*, ethyl 2-bromoisobutyrate),[30,31] thereby greatly enhancing the initiation efficiency and rate or, in other words, achieving both rapid and simultaneous chain initiation.

SI−ATRP of styrene was initiated from the bromophenyl groups of the TDBPA SAM atop the silicon surface in three different solvents, *i.e.*, toluene, cyclohexane, and *N*-hexane, respectively. Figure 2a shows the growth of PS brushes as a function of polymerization time. A linear increase in brush thickness *vs.* polymerization time was observed for each solvent. Nevertheless, toluene yielded the thickest brushes. The molecular weight (M_w) and polydispersity (PDI) of the PS brushes were obtained by degrafting the brushes using tetrabutyl ammonium fluoride according to a previously reported method[40] and characterized directly using gel permeation chromatography (GPC). Several representative GPC curves of the degrafted brushes are displayed in Figure S2 in the SI. Table S1 lists the molecular parameters of several PS brushes. All PS brushes have a PDI < 1.4.

For each brush, σ_p was determined according to eq 1[40]

$$\sigma_p = \frac{h_p \rho N_A}{M_n} \quad (1)$$

where ρ is approximated as the bulk density of PS (1.05 g cm^{-3}), h_p is the thickness of the dry brush, and N_A is Avogadro's number. Figure 2b shows a linear relationship between h_p and M_n, which implies uniform chain growth and negligible chain termination. By fitting the data in Figure 2b to eq 1, we calculated σ_p to be 0.69, 0.95, and 1.23 nm^{-2} for PS brushes polymerized in *N*-hexane, cyclohexane, and toluene, respectively. For PS brushes prepared in toluene, $\sigma_p^* \approx 0.85$, thus representing the synthesis of brushes with the highest grafting density reported to date with respect to the theoretical maximum; see Figure S1 in the SI. Each polymer chain in the brushes is hyperstretched and oriented in the direction normal to the film surface.

The dependence of σ_p on solvent is also intriguing. We found only minor deviations in M_n of brushes with the same reaction time but with different solvents as the reaction medium; see Table S1 in the SI. This observation suggests that the rate of polymerization was nearly independent of the solvent type. The difference in brush density, as a function of solvent, was then likely due to differences in the chain conformation states in solution, which influenced the steric hindrance for chain initiation.[41] More highly stretched chain conformations are favored in toluene, which is the best solvent for PS; see inset in Figure 2b. In contrast, the relatively poorer solvents of cyclohexane and *N*-hexane likely inhibited the growing brush from exploring its conformational space, thus promoting the formation of large coils that shielded the initiating sites at the surface (see inset in Figure 2a), resulting in a reduced overall brush density.

We then assessed the thermal stability of PS brushes as a function of brush density by measuring the T_g and thermal expansion *via* variable-temperature ellipsometry. Figure 3a plots the normalized thickness as a function of temperature for the ultrahigh grafting density brush, *i.e.*, σ_p = 1.23 nm^{-2}, for various thicknesses. As shown in Figure 3a, linear thermal expansion in both rubbery and glassy states was observed for all brushes. A tanh profile can describe well the transition between the expansion coefficients.[42] The transition point (T_g), width (w), and expansivities of the brush films were obtained by curving fitting the normalized thickness vs temperature profiles using a hyperbolic tangent function (eq 2)[42]

https://doi.org/10.1021/acsnano.0c09631
ACS Nano 2021, 15, 9568−9576

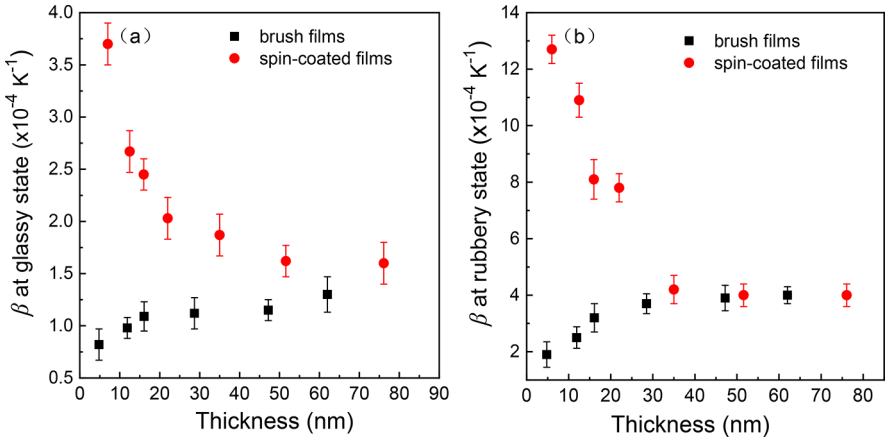

Figure 4. β in the (a) glassy and (b) rubbery states for PS ultradense brushes (σ_p = 1.23 nm^{-2}) and spin-cast films as a function of thickness. Error bars correspond to the standard deviation from at least three different measurements.

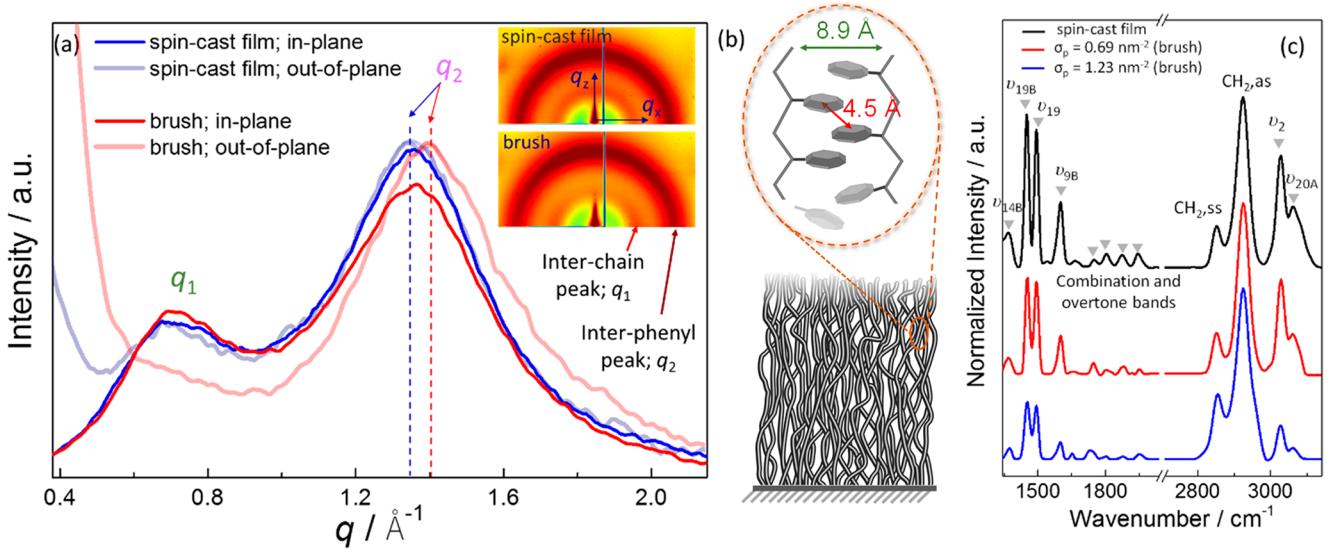

Figure 5. (a) 1D GIWAXS spectra and 2D pattern (inset) of a PS spin-cast film and brush (σ_p = 1.23 nm^{-2}) of similar thickness (40 ± 3 nm). (b) Schematic showing the ultradense grafting induced ordering of chains and phenyl groups and enhanced aromatic π–π stacking. (c) Infrared reflection absorption spectroscopy spectra (IRRAS) of PS spin-cast film and brushes. All peaks relevant to bond vibration in the phenyl ring were labeled by an inverted triangle. υ_{20A} and υ_2 come from the aromatic C–H stretching vibrations.[51] υ_{9B}, υ_{19B}, and υ_{14B} originate from carbon–carbon stretching in the aromatic ring.[51] CH_2,ss and CH_2,as represent the symmetric and asymmetric stretching vibrations of methylene groups in the backbone, respectively.[51] Except for the 1735 cm^{-1} peak, intensities of all the vibrations associated with phenyl rings were substantially reduced for the brushes. The reduction was more remarkable upon increasing the grafting density. We interpreted this band intensity reduction upon chain grafting as a result of denser phenyl–phenyl packing, as evidenced by GIWAXS data, which restricted the dipole moment of the phenyl-associated vibrations.

$$h(T) = w\left(\frac{M-G}{2}\right)\ln\left(\cosh\left(\frac{T-T_g}{w}\right)\right) + (T-T_g)\left(\frac{M+G}{2}\right) + c \quad (2)$$

where c is the film thickness at T_g, w is the width of the glass transition, and M and G are the dh/dT slope values for the rubbery and glassy states, respectively. The thermal expansion coefficient (β) was defined as the slope ($dh_p/h_p dT$) in each state. The values of T_g and w for the ultradense brush with various thicknesses are tabulated in Table S2 in the SI. The T_g increases remarkably (~35 K), while the width of the transition only shows marginal variations with a reduction in thickness.

Figure 3b plots T_g as a function of thickness for PS brushes with various σ_p measured at a heating rate of 2 K/min. For all values of σ_p, below a critical thickness ~60 nm, T_g increases with decreasing film thickness. The effect of thickness on T_g varied with σ_p, with the greatest change observed for σ_p = 1.23 nm^{-2}. For a 5 nm thick brush, T_g was 18, 27, and 36 K greater than the bulk value for brushes with σ_p = 0.69, 0.95, 1.23 nm^{-2}, respectively. The increases in the T_g of the ultradense brushes are strikingly large, especially when considered in the context of spin-cast PS films of similar thickness. The gray diamonds in Figure 3b reflect the behavior of spin-cast PS films. In stark contrast, ultrathin films of PS prepared by spin-casting show a tremendous reduction in T_g with decreasing film thickness due to free surface effects.[43−46] A 5 nm thick PS ultradense brush exhibits an ~75 K increment in T_g compared to a spin-cast film of similar thickness (~7 nm).

To probe the influence of grafting density, we plot T_g *vs.* σ_p at constant thickness for 5, 10, and 20 nm thick films in Figure 3c. For each film thickness, we observed a linear increase in T_g with increasing grafting density. Hence, denser brushes showed

https://doi.org/10.1021/acsnano.0c09631
ACS Nano 2021, 15, 9568−9576

greater kinetic stability. In line with these findings, a reduction in both rubbery and glassy state β was observed (Figure 4). The rubbery state β was reduced by ~55% compared to the bulk value and by ~87% compared to the corresponding thin film (Figure 4). Compared with the increasing trend of β for the spin-cast films[47] and PS brushes with $\sigma_p^* \approx 0.45$,[27] the β depression of the high-density brush ($\sigma_p^* = 0.85$) of thinner thickness is caused by the ultradense chain grafting that modifies molecular packing. The significantly increased T_g and depressed thermal expansion render the ultradense brush an ultrathin stable glassy film whose properties are less perturbed by temperature variations—a highly desirable trait for thin-film technologies.

The T_g of polymer brushes is determined by a complex interplay of various factors, such as the degree of chain stretching and film thickness. Recent work demonstrated that polymer brushes exhibit a distribution in local T_g, *i.e.*, higher T_g near the tethering point and lower T_g at the free surface.[29,48] Offsets between one another result in less significant variations in the average T_g.[12] In the case of PS brushes with σ_p of 0.33 nm^{-2}, the T_g of the brush was found to be invariant with thickness down to ~10 nm.[29] Yet, the ultradense brush films of PS show a tremendous increase in T_g with decreasing thickness.

Since T_g is sensitive to intermolecular interactions and packing, we probed the microstructure of the ultradense PS brush and spin-cast films using synchrotron grazing incidence wide-angle X-ray scattering (GIWAXS) (Figure 5a). The GIWAXS patterns of the spin-cast film consisted of two isotropic rings at $q_1 = 0.7$ Å^{-1} and $q_2 = 1.35$ Å^{-1} arising from the backbone-to-backbone correlation (interchain peak) and the $\pi-\pi$ interactions from phenyl groups in neighboring chains (interphenyl peak),[49,50] respectively. Notably, the GIWAXS patterns of the ultradense PS brush exhibited anisotropy, which is also visualized in the plot of scattering intensity *vs.* azimuthal angle (Figure S3 in the SI). The scattering intensity of the interchain peak (q_1) was greater in the in-plane direction (*i.e.*, along q_x), which suggested a preferentially perpendicular orientation of the backbone, as shown in Figure 5b. However, the intensity of the interphenyl peak (q_2) was stronger in the out-of-plane direction (*i.e.*, along q_z), which suggested the tendency of a parallel alignment of planar phenyl ring (Figure 5b). Moreover, an ~4% reduction of the phenyl−phenyl distance in the perpendicular direction was evident by a shift of the q_2 peak from 1.35 to 1.40 Å^{-1} in the out-of-plane spectra (see 1D spectra in Figure 5a), indicating closer phenyl−phenyl packing. The denser $\pi-\pi$ stacking also possibly resulted in a suppression of the dipole movement of bond vibration in the phenyl ring, as evidenced by a notable decrease of the corresponding IR peak intensities (Figure 5c). The hyper-stretched chain conformation and facilitated $\pi-\pi$ stacking, as evidenced by GIWAXS, reduce the ability of chain expansion along the thickness direction and cause the exceptional rise in T_g of the ultradense polymer brushes. The ultrastability of the brush films is therefore directly attributable to the ultradense brush morphology.

CONCLUSIONS

In this work, we reported the formation of ultradense PS brushes with a grafting density reaching ~85% of the theoretical maximum by combining the principles of self-assembly of initiators on substrate surfaces and SI−ATRP. The ultradense brushes, characterized by hyperefficient chain packing in the amorphous state, exhibited a significant enhancement in T_g and reduction in thermal expansivity, both signatures of ultrastability. We anticipate that besides the dramatic enhancement in thermal stability, the distinct morphological structure of ultradense brushes will endow polymeric systems with an array of enhanced physical properties (*e.g.*, mechanical and optical properties) in comparison to systems with a traditional random coil morphology. Such enhancements reinforce the idea of effective manipulation of material properties by changing how chains molecularly pack. In summary, the study provides fundamental insights into the thermal stability of dense polymer brushes. It also serves as a starting point for the experimental preparation and characterization of the ultradense polymer thin films with different structures and properties for diverse applications.

MATERIALS AND METHODS

Synthesis of TDBPA. *Materials.* Monodispersed atactic polystyrene (PS) (M_w = 168 kg mol^{-1}, PDI = 1.05) was purchased from Showa Denko K.K. in Japan (Shodex Standard). 11-Bromo-1-undecene (J&K Chemicals, 95%), 11-bromo-1-undecanol (J&K Chemicals, 98%), magnesium (Mg, Macklin), 1,2-dibromoethane (Aldrich, 99%), methyllithium (CH_3Li, 1.6 M solution in diethyl ether, J&K Chemicals), superdry methylene chloride (CH_2Cl_2, water content < 30 ppm, Aldrich), tetrahydrofuran (THF, Macklin, 99%), copper(I) iodide (CuI, J&K Chemicals, 98%), α-bromophenylacetic acid (Aldrich, 98%), *N*,*N*′-dicyclohexylcarbodiimide (DCC, Aldrich, 99%), 4-(*N*,*N*-dimethylamino)pyridine (DMAP, Aldrich, 99%), copper(I) bromide (CuBr, Aldrich, 98%), copper(II) bromide ($CuBr_2$, Aldrich, 99%), *N*,*N*,*N*′,*N*″,*N*″-pentamethyldiethyl-enetriamine (PMDETA, Aldrich, 99%), and platinum(0)-1,3-divinyl-1,1,3,3-tetramethylsiloxane complex in xylene (Karstedt's catalyst, Aldrich, 2% Pt), trichlorosilane ($HSiCl_3$, J&K Chemicals, 98%), tetrabutyl ammonium fluoride (TBAF, 1 M solution in THF, Aldrich), and isopropanol (Macklin, 99.5%) were used as received. Styrene (Aldrich, 99%) was purified by passing through an alumina column and distilled under reduced pressure.

Synthesis of the SI−ATRP Initiators (i.e., TDBPA). TDBPA was synthesized by three steps, as shown in Figure S4 of the SI. First, docos-21-en-1-ol (DEO) was prepared by a coupling reaction between 11-bromo-1-undecene and 11-bromo-1-undecanol using a Grignard reagent and copper iodide according to methods reported in refs 52 and 53. Then, an esterification reaction between hydroxyl groups on DEO and a carboxyl group on α-bromophenylacetic acid was processed to produce docos-21-en-1-yl 2-bromo-2-phenylacetate (DEBPA). Finally, a hydrosilylation reaction with trichlorosilane yielded a long-chain compound with a $-SiCl_3$ group capable of bonding to the silicon surface along with a highly active initiating group (*i.e.*, BPA), which would later be used to initiate ATRP.

Synthesis of Docos-21-en-1-ol (DEO). Magnesium turnings of 1.7 g and a freshly distilled THF of 2 mL were added into a 250 mL three-necked flask under nitrogen. A few drops of 1,2-dibromoethane were added into the system to activate the magnesium. A solution of 11-bromo-1-undecene (11.65 g) in THF (50 mL) was then added dropwise into the flask, and a moderate reflux was obtained just after a few minutes. The temperature in the system need not exceed 55 °C during the addition. The temperature was subsequently raised to 50 °C and maintained for 2 h, following a cooling to −78 °C. After 20 min at −78 °C, 0.38 g of CuI was added under a nitrogen stream. The mixture was maintained at −78 °C for another 10 min and then warmed to 0 °C. A deep purple color gradually appeared in the reaction solution. The system was then cooled to −78 °C again, and the protected 11-bromo-1-undecanol (10.28 g) in 50 mL of THF was added. Note that the −OH group of the bromo alcohol was protected upon reaction with CH_3Li, yielding the OLi compound. The mixture was kept stirred at −78 °C for 3 h before it was returned to room temperature (RT) and kept for 10 h. The reaction mixture was then hydrolyzed, and the upper organic layer was extracted three to five

https://doi.org/10.1021/acsnano.0c09631
ACS Nano 2021, 15, 9568−9576

times with diethyl ether. The combined organic fractions were washed subsequently with HCl (1 M), saturated $NaHCO_3$ aqueous solution, and water. The mixture solution was dried over anhydrous $MgSO_4$. The solvent was eliminated using the rotary evaporator under vacuum to obtain crude products. After they were precipitated using anhydrous acetone, the final products were collected by suction filtration and dried in a vacuum oven at 40 °C. ^{1}H NMR data in Figure S6 in the SI confirmed the structure of DEO. A yield of 70% was achievable.

Synthesis of Docos-21-en-1-yl 2-Bromo-2-phenylacetate (DEBPA). Docos-21-en-1-ol (18.47 g, 57 mmol), α-bromophenylacetic acid (10 g, 47 mmol), and DMAP (0.51 g, 4.2 mmol) were dissolved in 134 mL of dry DCM in a flask. DCC (10.7 g) was dissolved in 40 mL of dry DCM. Both solutions were cooled down to 0 °C in an ice bath. The DCC solution was then injected dropwise into the reaction system over 30 min. The reaction system was kept stirred at room temperature for 24 h and filtered to obtain raw products. The resulting solids were washed with DCM and then concentrated with rotary evaporation to get the crude product. The product was purified *via* silica column chromatography eluted using a 30:1 (v/v) hexane–ethyl acetate mixture. Upon removal of the solvent, docos-21-en-1-yl 2-bromo-2-phenylacetate (DEBPA) was obtained. ^{1}H NMR spectra shown in Figure S6 in the SI confirmed the successful synthesis of DEBPA.

Synthesis of 22-(Trichlorosilyl) Docosyl 2-Bromo-2-phenylacetate (TDBPA). To a dry flask were added 2.20 g of docos-21-en-1-yl 2-bromo-2-phenylacetate (DEBPA) and trichlorosilane (4.3 mL), followed by Karstedt catalyst (4 μL). At room temperature, the mixture was stirred for ∼24 h to complete the reaction. The reaction solution was filtered through a plug of silica gel in order to remove the catalyst. The excess solvents were removed. The compound was further purified by vacuum distillation at room temperature and at 2.0 × 10^{-2} mmHg. The compound needs to be stored in a drybox at 5 °C, when not in use. Structures of TDBPA were confirmed by H^{1}NMR spectra shown in Figure S6 of the SI.

Preparation of a Self-Assembled Monolayer (SAM) of TDBPA on the Si Surface. Silicon wafers were used as substrates and were cleaned by a "piranha" solution at 90 °C for 60 min, which allowed the formation of a thin native oxide layer. Self-assembled monolayers (SAMs) of TDBPA were prepared by immersing a clean silicon substrate with a thin native oxide layer into a 1.0 mM TDBPA toluene solution under nitrogen atmosphere for different time periods at room temperature. After sequential rinsing with chromatographically pure methylene chloride, isopropanol, acetone, distilled water, and chloroform, the samples were dried by a stream of clean nitrogen. The structure and properties of the samples were then characterized by AFM, ellipsometry, and SFG.

SI–ATRP for PS Brushes from the TDBPA SAM Surface. Polystyrene brushes of various grafting densities on planar Si wafers were prepared by SI–ATRP.[54] A degassed toluene solution (10 mL) containing CuBr (0.067 g), $CuBr_2$ (0.011 g), and PMDETA (0.11 mL) was prepared in a flask with stirring. Next, 5 mL of deinhibited styrene monomer was added into the flask, after which the TDBPA-SAM-covered Si wafers of 1 × 1 cm in size were added at RT. Growth of PS from the Si wafers (*i.e.*, the SI–ATRP process) was carried out at 90 °C under nitrogen. The thickness and M_w of the brushes were well-controlled by changing the reaction time. The resultant PS brushes atop the Si surfaces were washed with THF in a Soxhlet extractor for 24 h to remove the physically adsorbed chains, and a nitrogen stream was applied to dry the brush films.

Characterizations. The M_w and PDI of the brushes were determined *via* GPC of brushes degrafted from the silicon surfaces using TBAF as the degrafting reagent.[40] To degraft the brush chains, the Si wafers with PS brushes atop were placed into a 20 mL TBAF solution (0.04 M) in THF and incubated at 55 °C for 24 h. The solution was then concentrated to ∼1 mL. The reduced solution was filtered through polytetrafluoroethylene membranes with a pore size of 0.2 μm. The M_w and its distribution of the degrafted PS in the solution were measured at 35 °C by GPC (Waters Co., USA) equipped with a 1515 Isocratic HPLC Pump and a 2414 Refractive Index Detector operating with THF as the eluent. SFG spectroscopy (EKSPLA Co., Lithuania) with incident angles of 60 and 53° for the visible and IR laser beams, respectively, was used to detect the molecular structures and ordering at film surface.

The thickness of PS brushes and supported films atop the Si wafers was examined in air by an imaging ellipsometry (Accurion GmbH, Germany). The wavelength of the light beam for this measurement was fixed to be 658 nm, while the incidence angles were varied from 55 to 75°. The T_g and β of the PS brushes and films were evaluated by the thickness change upon the continuous heating process with a rate of 2 K/min using the Accurion ellipsometer at an incidence angle of 60°, equipped with an INSTEC heating state. During the measurements, we stopped the heating at 420–430 K, as the brush chains would detach from the substrate surface at elevated temperatures due to the entropic tensions that could possibly break the tethering bonds.[55,56] The T_g and β of the brushes were determined by fitting the thickness versus temperature relations with eq 2.

Infrared reflection absorption spectroscopy spectra (IRRAS) of PS spin-cast films and brushes was performed using a KSV NIMA system atop a thin gold-layer-covered Si substrate, as previously reported.[57] The incoming IR beam with an incidence angle of 76° interacted with the film and brushes at the substrate surface. The reflected beam was then guided into a detector to obtain the IR spectra. The spin-cast film was obtained by directly spin-coating a PS toluene solution atop the substrate surface, while the brush samples for IRRAS measurements were obtained by detaching a premade brush film from an Si surface and then transferring it to the gold-covered Si substrate.

GIWAXS measurements for the spin-cast and brush films were carried out at the Complex Materials Scattering (CMS) beamline with λ = 0.0918 nm and E = 13.5 keV at the National Synchrotron Light Source II (NSLS-II), Brookhaven National Laboratory. The 0.1° incident angle of X-ray, which is slightly above the critical angle of the total external reflection for PS (*i.e.*, 0.09°), was utilized, such that the overall structures over the entire film depth could be readily obtained. All experiments were conducted at room temperature under vacuum, and the exposure time of 200 s was chosen for the measurements.

ASSOCIATED CONTENT

Supporting Information

The Supporting Information is available free of charge at https://pubs.acs.org/doi/10.1021/acsnano.0c09631.

Grafting densities of PS and PMMA brushes documented in the literature; representative GPC traces of degrafted PS brushes; annular averaged intensity *vs.* azimuthal angle for PS films and brushes; synthetic route and H^1 NMR characterizations to TDBPA; structure parameters of the PS brushes; T_g and width of the glass transition (w) for the ultradense PS brushes (PDF)

AUTHOR INFORMATION

Corresponding Authors

Biao Zuo – *Department of Chemistry, Key Laboratory of Surface & Interface Science of Polymer Materials of Zhejiang Province and National Engineering Lab for Textile Fiber Materials and Processing Technology (Zhejiang), Zhejiang Sci-Tech University, Hangzhou 310018, China;* orcid.org/0000-0002-4921-8823; Phone: +86 571 86843639; Email: chemizuo@zstu.edu.cn

Xinping Wang – *Department of Chemistry, Key Laboratory of Surface & Interface Science of Polymer Materials of Zhejiang Province, Zhejiang Sci-Tech University, Hangzhou 310018, China;* orcid.org/0000-0002-9269-3275; Phone: +86 571 86843600; Email: wxinping@zstu.edu.cn

Rodney D. Priestley – *Department of Chemical and Biological Engineering and Princeton Institute for the Science and Technology of Materials, Princeton University, Princeton,*

https://doi.org/10.1021/acsnano.0c09631
ACS Nano 2021, 15, 9568–9576

New Jersey 08544, United States; orcid.org/0000-0001-6765-2933; Phone: +1 609 258 5721; Email: rpriestl@princeton.edu

Authors

Cheng Li − *Department of Chemistry, Key Laboratory of Surface & Interface Science of Polymer Materials of Zhejiang Province, Zhejiang Sci-Tech University, Hangzhou 310018, China*

Quanyin Xu − *Department of Chemistry, Key Laboratory of Surface & Interface Science of Polymer Materials of Zhejiang Province, Zhejiang Sci-Tech University, Hangzhou 310018, China; Department of Chemical and Biological Engineering, Princeton University, Princeton, New Jersey 08544, United States*

Katelyn Randazzo − *Department of Chemical and Biological Engineering, Princeton University, Princeton, New Jersey 08544, United States*

Naisheng Jiang − *School of Materials Science and Engineering, University of Science and Technology Beijing, Beijing 100083, China*

Complete contact information is available at: https://pubs.acs.org/10.1021/acsnano.0c09631

Notes

The authors declare no competing financial interest.

ACKNOWLEDGMENTS

B.Z. and X.W. thank the support from the National Natural Science Foundation of China (21973083, 22011530456, and 21674100). R.D.P. gratefully acknowledges the National Science Foundation (NSF) Materials Research Science and Engineering Center Program through the Princeton Center for Complex Materials (DMR-1420541 and 2011750) and through CBET-1706012. The authors also thank Ruipeng Li and Masafumi Fukuto for assisting the synchrotron X-ray scattering measurements. This research used the Complex Materials Scattering (CMS/11-BM) beamline, operated by the National Synchrotron Light Source II at Brookhaven National Laboratory, which is supported by the U.S. Department of Energy, Office of Science, Office of Basic Energy Sciences, under Contract No. DE-SC0012704.

REFERENCES

(1) Mansky, P.; Liu, Y.; Huang, E.; Russell, T. P.; Hawker, C. Controlling Polymer-Surface Interactions with Random Copolymer Brushes. *Science* **1997**, *275*, 1458−1460.

(2) Chen, W.-L.; Cordero, R.; Tran, H.; Ober, C. K. 50th Anniversary Perspective: Polymer Brushes: Novel Surfaces for Future Materials. *Macromolecules* **2017**, *50*, 4089−4113.

(3) Tsujii, Y.; Ohno, K.; Yamamoto, S.; Goto, A.; Fukuda, T. Structure and Properties of High-Density Polymer Brushes Prepared by Surface-Initiated Living Radical Polymerization. *Adv. Polym. Sci.* **2006**, *197*, 1−45.

(4) Milner, S. T. Polymer Brushes. *Science* **1991**, *251*, 905−914.

(5) Yamamoto, S.; Tsujii, Y.; Fukuda, T. Glass Transition Temperatures of High-Density Poly (methyl Methacrylate) Brushes. *Macromolecules* **2002**, *35*, 6077−6079.

(6) Tranchida, D.; Sperotto, E.; Chateauminois, A.; Schönherr, H. Entropic Effects on the Mechanical Behavior of Dry Polymer Brushes during Nanoindentation by Atomic Force Microscopy. *Macromolecules* **2011**, *44*, 368−374.

(7) Klein, J.; Kumacheva, E.; Mahalu, D.; Perahia, D.; Fetters, L. J. Reduction of Frictional Forces between Solid Surfaces Bearing Polymer Brushes. *Nature* **1994**, *370*, 634−636.

(8) Urayama, K.; Yamamoto, S.; Tsujii, Y.; Fukuda, T.; Neher, D. Elastic Properties of Well-Defined, High-Density Poly (methyl Methacrylate) Brushes Studied by Electromechanical Interferometry. *Macromolecules* **2002**, *35*, 9459−9465.

(9) Devaux, C.; Cousin, F.; Beyou, E.; Chapel, J. P. Low Swelling Capacity of Highly Stretched Polystyrene Brushes. *Macromolecules* **2005**, *38*, 4296−4300.

(10) Michalek, L.; Barner, L.; Barner-Kowollik, C. Polymer on Top: Current Limits and Future Perspectives of Quantitatively Evaluating Surface Grafting. *Adv. Mater.* **2018**, *30*, 1706321.

(11) Yoshikawa, C.; Goto, A.; Tsujii, Y.; Fukuda, T.; Yamamoto, K.; Kishida, A. Fabrication of High-Density Polymer Brush on Polymer Substrate by Surface-Initiated Living Radical Polymerization. *Macromolecules* **2005**, *38*, 4604−4610.

(12) He, G. L.; Merlitz, H.; Sommer, J. U.; Wu, C. X. Polymer Brushes near the Crystallization Density. *Eur. Phys. J. E: Soft Matter Biol. Phys.* **2007**, *24*, 325−330.

(13) Lai, P. Y.; Halperin, A. Polymer Brush at High Coverage. *Macromolecules* **1991**, *24*, 4981−4982.

(14) Shim, D. F. K.; Cates, M. E. Finite Extensibility and Density Saturation Effects in the Polymer Brush. *J. Phys. (Paris)* **1989**, *50*, 3535−3551.

(15) Zhou, T.; Qi, H.; Han, L.; Barbash, D.; Li, C. Y. Towards Controlled Polymer Brushes *via* a Self-Assembly-Assisted-Grafting-To Approach. *Nat. Commun.* **2016**, *7*, 11119.

(16) Barbey, R.; Lavanant, L.; Paripovic, D.; Schüwer, N.; Sugnaux, C.; Tugulu, S.; Klok, H.-A. Polymer Brushes *via* Surface-Initiated Controlled Radical Polymerization: Synthesis, Characterization, Properties, and Applications. *Chem. Rev.* **2009**, *109*, 5437−5527.

(17) Prucker, O.; Rühe, J. Polymer Layers through Self-Assembled Monolayers of Initiators. *Langmuir* **1998**, *14*, 6893−6898.

(18) Ramakrishnan, A.; Dhamodharan, R.; Rühe, J. Controlled Growth of PMMA Brushes on Silicon Surfaces at Room Temperature. *Macromol. Rapid Commun.* **2002**, *23*, 612−616.

(19) Wei, W.; Balamurugan, A.; Dwyer, J. H.; Gopalan, P. Substrate-Independent Approach to Dense Cleavable Polymer Brushes by Nitroxide-Mediated Polymerization. *ACS Macro Lett.* **2018**, *7*, 100−104.

(20) Swallen, S. F.; Kearns, K. L.; Mapes, M. K.; Kim, Y. S.; Mcmahon, R. J.; Ediger, M. D.; Wu, T.; Yu, L.; Satija, S. Organic Glasses with Exceptional Thermodynamic and Kinetic Stability. *Science* **2007**, *315*, 353−356.

(21) Guo, Y.; Morozov, A.; Schneider, D.; Chung, J. W.; Zhang, C.; Waldmann, M.; Yao, N.; Fytas, G.; Arnold, C. B.; Priestley, R. D. Ultrastable Nanostructured Polymer Glasses. *Nat. Mater.* **2012**, *11*, 337−343.

(22) Ediger, M. D. Perspective: Highly Stable Vapor-Deposited Glasses. *J. Chem. Phys.* **2017**, *147*, 210901.

(23) Berthier, L.; Ediger, M. D. Facets of Glass Physics. *Phys. Today* **2016**, *69* (1), 40−46.

(24) Milner, S. T.; Witten, T. A.; Cates, M. E. Theory of the Grafted Polymer Brush. *Macromolecules* **1988**, *21*, 2610−2619.

(25) de Gennes, P. G. Conformations of Polymers Attached to an Interface. *Macromolecules* **1980**, *13*, 1069−1075.

(26) Fytas, G.; Anastasiadis, S. H.; Seghrouchni, R.; Vlassopoulos, D.; Li, J.; Factor, B. J.; Theobald, W.; Toprakcioglu, C. Probing Collective Motions of Terminally Anchored Polymers. *Science* **1996**, *274*, 2041−2044.

(27) Zuo, B.; Zhang, S.; Niu, C.; Zhou, H.; Sun, S.; Wang, X. Grafting Density Dominant Glass Transition of Dry Polystyrene Brushes. *Soft Matter* **2017**, *13*, 2426−2436.

(28) Keddie, J. L.; Jones, R. A. L. Glass Transition Behavior in Ultra-Thin Polystyrene Films. *Isr. J. Chem.* **1995**, *35*, 21−26.

(29) Lan, T.; Torkelson, J. M. Substantial Spatial Heterogeneity and Tunability of Glass Transition Temperature Observed with Dense

Polymer Brushes Prepared by ARGET ATRP. *Polymer* **2015**, *64*, 183−192.
(30) Yan, J.; Pan, X.; Schmitt, M.; Wang, Z.; Bockstaller, M. R.; Matyjaszewski, K. Enhancing Initiation Efficiency in Metal-Free Surface-Initiated Atom Transfer Radical Polymerization (SI−ATRP). *ACS Macro Lett.* **2016**, *5*, 661−665.
(31) Tang, W.; Matyjaszewski, K. Effects of Initiator Structure on Activation Rate Constants in ATRP. *Macromolecules* **2007**, *40*, 1858−1863.
(32) Bain, C. D.; Troughton, E. B.; Tao, Y. T.; Evall, J.; Whitesides, G. M.; Nuzzo, R. G. Formation of Monolayer Films by the Spontaneous Assembly of Organic Thiols from Solution onto Gold. *J. Am. Chem. Soc.* **1989**, *111*, 321−335.
(33) Shen, Y. R. Surface Properties Probed by Second-Harmonic and Sum-Frequency Generation. *Nature* **1989**, *337*, 519−525.
(34) Zuo, B.; Zhou, H.; Davis, M. J.; Wang, X.; Priestley, R. D. Effect of Local Chain Conformation in Adsorbed Nanolayers on Confined Polymer Molecular Mobility. *Phys. Rev. Lett.* **2019**, *122*, 217801.
(35) Walker, R. A.; Gruetzmacher, J. A.; Richmond, G. L. Phosphatidylcholine Monolayer Structure at a Liquid-Liquid Interface. *J. Am. Chem. Soc.* **1998**, *120*, 6991−7003.
(36) Kojio, K.; Takahara, A.; Omote, K.; Kajiyama, T. Molecular Aggregation State of *N*-octadecyltrichlorosilane Monolayers Prepared by the Langmuir and Chemisorption Methods. *Langmuir* **2000**, *16*, 3932−3936.
(37) Hayes, R.; Watson, G. W.; Willock, D. J. Simulation of the Structure of Organosilane Film Coatings. *Mol. Simul.* **2006**, *32*, 1095−1101.
(38) Ulman, A. Formation and Structure of Self-Assembled Monolayers. *Chem. Rev.* **1996**, *96*, 1533−1554.
(39) Azzam, W.; Fuxen, C.; Birkner, A.; Rong, H.-T.; Buck, M.; Wöll, C. Coexistence of Different Structural Phases in Thioaromatic Monolayers on Au(111). *Langmuir* **2003**, *19*, 4958−4968.
(40) Patil, R. R.; Turgman-Cohen, S.; Šrogl, J.; Kiserow, D.; Genzer, J. Direct Measurement of Molecular Weight and Grafting Density by Controlled and Quantitative Degrafting of Surface-Anchored Poly(methyl Methacrylate). *ACS Macro Lett.* **2015**, *4*, 251−254.
(41) Feng, W.; Chen, R.; Brash, J. L.; Zhu, S. Surface-Initiated Atom Transfer Radical Polymerization of Oligo (ethylene Glycol) Methacrylate: Effect of Solvent on Graft Density. *Macromol. Rapid Commun.* **2005**, *26*, 1383−1388.
(42) Dalnoki-Veress, K.; Forrest, J. A.; Murray, C.; Gigault, C.; Dutcher, J. R. Molecular Weight Dependence of Reductions in the Glass Transition Temperature of Thin, Freely Standing Polymer Films. *Phys. Rev. E: Stat. Phys., Plasmas, Fluids, Relat. Interdiscip. Top.* **2001**, *63*, 031801.
(43) Chai, Y.; Salez, T.; Mcgraw, J. D.; Benzaquen, M.; Dalnoki-Veress, K.; Raphaël, E.; Forrest, J. A. A Direct Quantitative Measure of Surface Mobility in a Glassy Polymer. *Science* **2014**, *343*, 994−998.
(44) Yang, Z.; Fujii, Y.; Lee, F. K.; Lam, C.-H.; Tsui, O. K. C. Glass Transition Dynamics and Surface Layer Mobility in Unentangled Polystyrene Films. *Science* **2010**, *328*, 1676−1679.
(45) Priestley, R. D.; Ellison, C. J.; Broadbelt, L. J.; Torkelson, J. M. Structural Relaxation of Polymer Glasses at Surfaces, Interfaces, and in between. *Science* **2005**, *309*, 456−459.
(46) Paeng, K.; Swallen, S. F.; Ediger, M. D. Direct Measurement of Molecular Motion in Freestanding Polystyrene Thin Films. *J. Am. Chem. Soc.* **2011**, *133*, 8444−8447.
(47) Xu, Q.; Zhu, N.; Fang, H.; Wang, X.; Priestley, R. D.; Zuo, B. Decoupling Role of Film Thickness and Interfacial Effect on Polymer Thin Film Dynamics. *ACS Macro Lett.* **2021**, *10*, 1−8.
(48) Askar, S.; Li, L.; Torkelson, J. M. Polystyrene-Grafted Silica Nanoparticles: Investigating the Molecular Weight Dependence of Glass Transition and Fragility Behavior. *Macromolecules* **2017**, *50*, 1589−1598.
(49) López-Barrón, C. R.; Zhou, H.; Younker, J. M.; Mann, J. A. Molecular Structure, Chain Dimensions, and Linear Rheology of Poly(4-Vinylbiphenyl). *Macromolecules* **2017**, *50*, 9048−9057.
(50) Mitchell, G. R.; Windle, A. H. Structure of Polystyrene Glasses. *Polymer* **1984**, *25*, 906−920.
(51) Olmos, D.; Martin, E. V.; Gonzalez-Benito, J. New Molecular-Scale Information on Polystyrene Dynamics in PS and PS−$BaTiO_3$ Composites from FTIR Spectroscopy. *Phys. Chem. Chem. Phys.* **2014**, *16*, 24339.
(52) Derguini-Boumechal, F.; Linstrumelle, G. Syntheses of Alkenes from Vinylic Grignard Reagents Activated by Copper Salts. *Tetrahedron Lett.* **1976**, *17*, 3225−3226.
(53) Dinh, D. H.; Vellutini, L.; Bennetau, B.; Dejous, C.; Rebiere, D.; Pascal, É.; Moynet, D.; Belin, C.; Desbat, B.; Labrugere, C.; et al. Route to Smooth Silica-Based Surfaces Decorated with Novel Self-Assembled Monolayers (SAMs) Containing Glycidyl-Terminated Very Long Hydrocarbon Chains. *Langmuir* **2009**, *25*, 5526−5535.
(54) Matyjaszewski, K.; Miller, P. J.; Shukla, N.; Immaraporn, B.; Gelman, A.; Luokala, B. B.; Siclovan, T. M.; Kickelbick, G.; Vallant, T.; Hoffmann, H.; et al. Polymers at Interfaces: Using Atom Transfer Radical Polymerization in the Controlled Growth of Homopolymers and Block Copolymers from Silicon Surfaces in the Absence of Untethered Sacrificial Initiator. *Macromolecules* **1999**, *32*, 8716−8724.
(55) Sheiko, S. S.; Sun, F. C.; Randall, A.; Shirvanyants, D.; Rubinstein, M.; Lee, H.; Matyjaszewski, K. Adsorption-Induced Scission of Carbon-Carbon Bonds. *Nature* **2006**, *440*, 191−194.
(56) Sheiko, S. S.; Panyukov, S.; Rubinstein, M. Bond Tension in Tethered Macromolecules. *Macromolecules* **2011**, *44*, 4520−4529.
(57) Jin, T.; Zha, H.; Randazzo, K.; Zuo, B.; Priestley, R. D.; Wang, X. Local Disorder Facilitates Chain Stretching in Crowded Polymer Brushes. *J. Phys. Chem. Lett.* **2020**, *11*, 7814−7818.

https://doi.org/10.1021/acsnano.0c09631
ACS Nano 2021, 15, 9568−9576